JOURNAL OF GUIDANCE, CONTROL, AND DYNAMICS
Vol. 34, No. 4, July–August 2011

Trajectory Prediction for Light Aircraft

Urban Maeder,* Manfred Morari, and Thomas Ivar Baumgartner
ETH Zurich, 8000 Zurich, Switzerland

DOI: 10.2514/1.52124

In this paper, a novel algorithm for estimation, filtering, and prediction of trajectories of light aircraft and gliders based on Global Positioning System measurements is introduced. The algorithm uses interacting-multiple-model filters to detect specific maneuvers such as turning, circling, or straight flight. An integrated wind model allows for quick estimation of the local wind field and helps to achieve consistently good prediction accuracy in windy conditions. The algorithm is shown to perform well compared with legacy algorithms currently used in a collision avoidance system.

Nomenclature

A	=	matrix with m rows and n columns, $\in \mathbb{R}^{m\times n}$
a_{ij}	=	element of A at row i and column j
$I_{n\times n}$	=	identity matrix of dimension n
k	=	discrete-time index, e.g., $f(k+1) := f(t+T)$
$\mathbb{R}$	=	set of real numbers
$\mathbb{R}^{m\times n}$	=	set of matrices with m rows and n columns containing real elements
r	=	scalar, $\in \mathbb{R}$
T	=	sampling time
t	=	time
$\boldsymbol{x}$	=	vector containing n real elements, $\in \mathbb{R}^{n\times 1}$, with $[x_1, \ldots, x_n]^T$
$0_{n\times m}$	=	matrix where each entry is 0
$1_{n\times m}$	=	matrix where each entry is 1

I. Introduction

MIDAIR collisions are a prominent problem in general aviation. It is estimated that about 20 such collisions occur worldwide each year, with about one-third of the involved aircraft being gliders [1]. Light aircraft often operate under visual flight rules in uncontrolled airspace. Every pilot is responsible for looking out carefully, detecting other traffic, and performing evasive maneuvers, if necessary. This paradigm is known as the *see-and-avoid* principle.

It is well known that the see-and-avoid principle has limitations, mostly due to human factors [2]. For instance, converging aircraft often cannot be seen by the pilot, since they appear static or may be camouflaged by the background. For gliders, the situation is particularly severe,due to their small cross section and their tendency to gather in lifting air masses such as thermals.

In commercial aviation, the development of collision avoidance systems (CAS) goes back to the 1950s; solutions are well-established and mandated by aviation authorities. These systems cannot be easily integrated into light aircraft, however, due to their high cost, power consumption, and bulkiness. Moreover, they do not take into consideration the highly dynamic flight patterns of light aircraft. Consequently, specific commercial systems for light aircraft have been developed recently.

FLARM® is a Global Positioning System (GPS)-based cooperative CAS introduced in 2004. It has proven to be reliable, easy to install and use, and very cost-effective. With an installation base of over 15,000 units in gliders and light aircraft, it has evolved to be the de facto standard of CAS in general aviation, complementing transponder-based services. FLARM uses a GPS receiver to determine its own position. It then computes a prediction of the future flight path, which is broadcast regularly using a digital radio transceiver. Other aircraft equipped with a compatible device may receive these data, process them, and issue collision warnings to the pilot, if necessary. Unlike other CAS, no recommendation is given on how to resolve the situation; the pilot needs to make his own decision. The system also serves as a traffic information system, indicating traffic far away with no risk of collision, thus increasing the situational awareness of the pilot, allowing him to avoid dangerous situations before they arise.

The accuracy of the trajectory prediction is of paramount importance for the performance of the system. If the accuracy is low, alarms have to be issued more often in order to avoid false negatives (i.e., no alarm is issued, even though there is a danger). This will in turn lead to a large number of nuisance alarms (false positives, i.e., an alarm is issued even though there is no danger), which reduce the situational awareness by unnecessarily increasing the work load of the pilot. Also, his confidence in the system will be lowered, which in turn may lead to him ignoring it or turning it off entirely. By increasing the prediction accuracy, the number of nuisance alarms can be reduced while keeping the number of false negatives low, thus yielding a more effective system.

Compared with commercial airplanes, the maneuverability of light aircraft is much higher. Moreover, typical movement patterns of aircraft flying in uncontrolled airspace are more complex, since there are fewer restrictions and the pilots fly manually instead of using the autopilot. Gliders, in particular, often perform seemingly erratic maneuvers, e.g., during the search for thermals. Stable flight patterns such as straight flight, circling in thermals, hang soaring, or contour flight may last for only a few seconds or up to a few minutes. Thus, a fast-adapting prediction algorithm is required. Moreover, unlike with commercial aircraft, wind can significantly influence the flight path of light aircraft. For the prediction algorithm to yield accurate trajectory predictions, it must deal with wind.

The trajectory prediction algorithm currently used by FLARM has been found to perform well in practice. However, it suffers from two problems: First, it does not provide a model for maneuvers. This typically leads to problems when an aircraft is flying straight, since even small course corrections will cause the prediction algorithm to assume that the aircraft is turning, yielding nuisance alerts, e.g., while overtaking or formation-flying. Second, it does not incorporate a wind estimate, which leads to degraded performance in windy conditions.

II. Preliminaries

This section provides a brief overview of the proposed method and introduces the basic concepts and algorithms applied in this work.

Presented at the 28th IEEE/AIAA Digital Avionics Systems Conference, Orlando, FL, 25–29 October 2009; received 22 August 2010; revision received 17 December 2010; accepted for publication 27 January 2011.

*Automatic Control Laboratory (Corresponding Author).

A. Coordinate Frames

The FLARM system uses a GSP receiver to determine the position of the aircraft. The position measurements are provided in the WGS-84 reference frame, consisting of latitude angle, longitude angle, and altitude above a standard ellipsoid. This reference frame is well suited for expressing global positions on Earth, but it is cumbersome for local computations. Since the distances relevant for collision avoidance are small compared with the Earth's radius, a local planar approximation can be used. We thus transform the GPS measurements into a local orthonormal coordinate frame, where the principal axes are aligned with the north, east, and down (NED) axes. Note that the choice of the down axis is purely by convention, to obtain a right-handed coordinate frame. Computations can be performed in this local frame with sufficient precision. The origin of the local frame is chosen to lie at the center of the aircraft at each time instant, which allows for several simplifications in the algorithm in terms of computational complexity. The velocity measurements also provided by the GPS receiver are already given in the NED frame and can thus be used directly.

B. Algorithm Overview

Figure 1 depicts the structure of the proposed algorithm. It comprises three stages: state estimation, maneuver detection, and prediction. The GPS receiver provides position and velocity measurements (each in three dimensions), and the RF transmitter is used to broadcast the computed trajectory to other devices.

In the first stage, the state of motion of the aircraft is inferred from past measurements. The interacting-multiple-model (IMM) filter algorithm is employed including a model of the local wind field. The second stage uses the results of the first stage to provide an estimate of the likelihood that some maneuver is currently being performed. A set of very simple behavioral models is used to capture most relevant situations. The third stage extrapolates the estimates produced by the first two stages to yield a predicted trajectory over the next 20 s. The current maneuver and the wind estimate are included in the extrapolation.

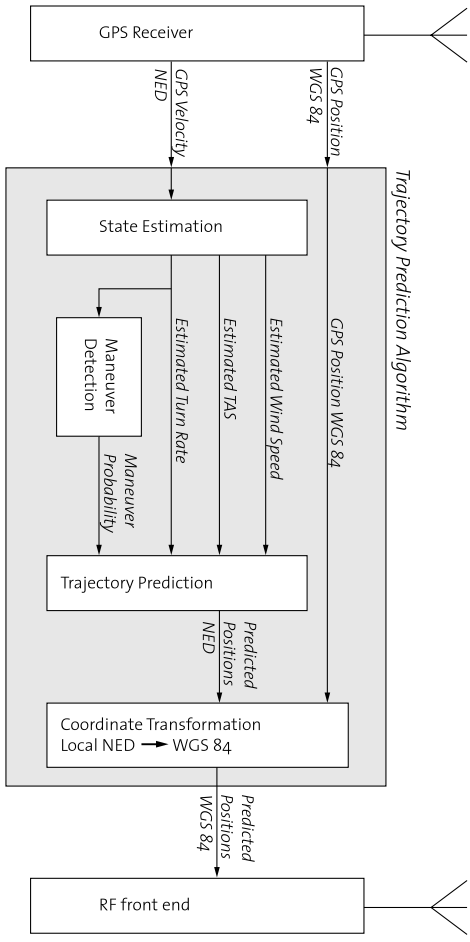

Fig. 1 Structure of the trajectory prediction algorithm.

C. Extended Kalman Filtering

The goal of state estimation, in general, is to infer the value of a quantity of interest from indirect and inaccurate measurement [3]. The extended Kalman filter (EKF) is a standard technique for the estimation of nonlinear systems of the form in Eq. (1). We briefly present the EKF algorithm here; for a thorough discussion, the reader is referred to the abundant literature available on the subject (e.g., [3–5]).

We consider autonomous discrete-time state-space models of the form

$$\boldsymbol{x}(k+1) = f(\boldsymbol{x}(k), \boldsymbol{w}(k)), \qquad \boldsymbol{y}(k) = h(\boldsymbol{x}(k)) + \boldsymbol{v}(k) \tag{1}$$

where $\boldsymbol{x}(k)$ is the state vector, $\boldsymbol{y}(k)$ is the vector of measurements, $f(\cdot,\cdot)$ and $h(\cdot)$ are nonlinear smooth functions, and $\boldsymbol{v}(k)$ and $\boldsymbol{w}(k)$ are unknown disturbances. We assume $\boldsymbol{w}(k)$ and $\boldsymbol{v}(k)$ to be multivariate white Gaussian noise vectors with

$$E[\boldsymbol{w}(k)\boldsymbol{w}(k)^T] = Q(k) \tag{2}$$

$$E[\boldsymbol{v}(k)\boldsymbol{v}(k)^T] = R(k) \tag{3}$$

$$E[\boldsymbol{w}(k)\boldsymbol{v}(k)^T] = 0 \tag{4}$$

Let $\hat{\boldsymbol{x}}(j|k)$ denote the estimate of the state vector for time j given all measurements up to time k, and let the real state $\boldsymbol{x}(k)$ admit a normal distribution with $\boldsymbol{x}(k) \sim \mathcal{N}(\hat{\boldsymbol{x}}(k|k), P(k|k))$. The EKF comprises two stages: prediction and update. The prediction stage updates the state and covariance estimates; it is given by

$$\hat{\boldsymbol{x}}(k|k-1) = f(\hat{\boldsymbol{x}}(k-1|k-1), 0) \tag{5a}$$

$$P(k|k-1) = F_x P(k-1|k-1) F_x^T + F_w Q(k) F_w^T \tag{5b}$$

where $F_x := (\partial/\partial \boldsymbol{x}) f(\hat{\boldsymbol{x}}(k-1|k-1), 0)$ denotes the Jacobian of f with respect to $\boldsymbol{x}$ evaluated at $\boldsymbol{x} = \hat{\boldsymbol{x}}(k-1|k-1)$, $\boldsymbol{w} = 0$, and $F_w := (\partial/\partial \boldsymbol{w}) f(\hat{\boldsymbol{x}}(k-1|k-1), 0)$ denotes the Jacobian with respect to $\boldsymbol{w}$ evaluated at the same point.

In the update stage, the measurements of time k are introduced, i.e.,

$$\hat{z}(k) = \boldsymbol{y}(k) - h(\hat{\boldsymbol{x}}(k|k-1)) \tag{6a}$$

$$S = H_x P(k|k-1) H_x^T + R(k) \tag{6b}$$

$$K = P(k|k-1) H_x^T S^{-1} \tag{6c}$$

$$\hat{\boldsymbol{x}}(k|k) = \hat{\boldsymbol{x}}(k|k-1) + K\hat{z}(k) \tag{6d}$$

$$P(k|k) = P(k|k-1) + K\hat{z}(k)K^T \tag{6e}$$

where $H_x := (\partial/\partial \boldsymbol{x}) h(\hat{\boldsymbol{x}}(k|k-1))$ denotes the Jacobian of h with respect to $\boldsymbol{x}$ evaluated at $\boldsymbol{x} = \hat{\boldsymbol{x}}(k|k-1)$.

D. Interacting-Multiple-Model Filtering

The IMM filter is an extension of other filter methods, such as the Kalman filter and EKF. It assumes that at any time instant, the system obeys one of a finite set of modes, and it contains one filter for every mode [3,6–9]. We discuss only the IMM based on EKF here, where the system is described by

$$\boldsymbol{x}_j(k+1) = f_j(\boldsymbol{x}_j(k), \boldsymbol{w}_j(k)), \qquad \boldsymbol{y}(k) = h_j(\boldsymbol{x}_j(k)) + \boldsymbol{v}(k) \quad (7)$$

where $j = 1, \ldots, r$, and $r \in \mathbb{N}$ is the number of modes. The currently active mode is not measurable and thus has to be inferred from measurement data. The system may switch from one mode to another with a given transition probability. Hence, the IMM filter needs to keep an estimate not only of the state vector (as in the EKF), but also of the probability that the system is in a given mode. The IMM achieves this by containing a distinct EKF for every mode and appropriately mixing the state vectors of each individual EKF.

Let $M_j(k)$ denote the event that mode j is active during the kth sampling period. Mode switches are modeled as a hidden Markov chain, where it is assumed that the transition probabilities are known, i.e., the probability to switch from mode i to j is given by

$$p_{ij} = P(M_j(k)|M_i(k-1)) \quad (8)$$

and is independent of the state vector. The IMM filter uses r underlying EKFs producing state and covariance estimates $\hat{\boldsymbol{x}}_j(k|k)$ and $P_k(k|k)$. Additionally, it computes the probability that the system is in mode j:

$$\mu_j(k|k) = P(M_j(k)|Z(k)) \quad (9)$$

where $Z(k)$ denotes the cumulative set of measurements up to time k. Furthermore, the IMM provides mixed versions of the state and covariance estimates:

$$\hat{\boldsymbol{x}}(k|k) = \sum_{j=1}^{r} \mu_j(k)\hat{\boldsymbol{x}}_j(k|k) \quad (10)$$

$$P(k|k) = \sum_{j=1}^{r} \mu_j(k)[P_j(k|k) + ((\hat{\boldsymbol{x}}_j(k|k) - \hat{\boldsymbol{x}}(k|k))((\hat{\boldsymbol{x}}_j(k|k) - \hat{\boldsymbol{x}}(k|k))^T)] \quad (11)$$

For details of the algorithm, the reader is referred to [3].

III. State Estimation

This section describes the first stage of the algorithm. The outputs produced by this stage are used in all subsequent stages; hence, achieving good dynamic performance in this stage is critical.

Estimation algorithms such as the EKF or IMM filters allow for embedding a dynamic model of the underlying process, thus leading to a superior performance when compared with model-less methods. Model-based estimation of the state of an aircraft has been discussed widely in the literature, mainly in the context of air traffic control (ATC) and air defense. In ATC, radar measurements are used to accurately track an aircraft; determine parameters such as speed, heading, or rate of climb; and provide the operator with these data. Similarly, air defense systems use radar tracking to determine the velocity vector and the distance to the aircraft so as to compute the correct lead angles for firing.

The accuracy of an estimation algorithm depends, to a large extent, on how well the embedded model matches the real dynamics [10]. A variety of models have been proposed, mostly falling into either of two categories: uniform motion (UM) and coordinated turn (CT) models [11–16]. In the uniform motion model, it is assumed the aircraft does not turn or change velocity. This model is often accurate enough for ATC applications, where the aircraft mostly fly with constant heading and perform turns only occasionally. In the coordinated turn model, a variable turn rate is introduced, thus yielding better estimates for maneuvering aircraft, but also rendering the filter more susceptible to noise.

The UM model is effective at rejecting disturbances in straight flight, whereas the CT model provides quicker convergence rates for dynamic maneuvers. Since IMM filters allow integration of both the CT and the UT models, they effectively combine the advantages of both models. Algorithms implementing IMM have thus been shown to perform better than pure EKFs in this class of problems [7–9,17]. A survey on IMM and its applications can be found in [3,18]. In this text, both UM and CT models are employed.

A. Aircraft Equations of Motion

In commercial aviation, the velocity of aircraft typically is large compared with wind speeds, and the aircraft perform only slow maneuvers with moderate turn rates. Wind is thus usually modeled as white noise added to the velocity [14], which is sufficiently accurate for radar tracking applications. For light aircraft, wind is more important, due to lower airspeeds and higher maneuver dynamics, since it can lead to significant displacement when turning (see Fig. 2). To this end, we employ an augmented dynamical model including the local wind field.

Denote $\boldsymbol{v} = [\, v_N \quad v_E \quad v_D \,]^T$ as the local velocity of the aircraft, ω is its rate of turn, and $\boldsymbol{d} = [\, d_N \quad d_E \,]^T$ is the local wind field. The vertical wind (e.g., lift, sink) is ignored, since the accuracy of the GPS is too low compared with vertical wind speeds. The dynamics of motion are given by

$$\dot{v}_N = -\omega v_E, \qquad \dot{v}_E = \omega v_N, \qquad \dot{v}_D = 0$$
$$\dot{\omega} = 0, \qquad \dot{d}_N = 0, \qquad \dot{d}_E = 0 \quad (12)$$

The measurements are given by

$$\boldsymbol{y}(t) = \begin{bmatrix} v_N(t) + d_N(t) \\ v_E(t) + d_E(t) \\ v_D(t) \end{bmatrix} \quad (13)$$

Let the combined state vector be given by

$$\boldsymbol{x} = [\, v_N \quad v_E \quad v_D \quad \omega \quad d_N \quad d_E \,]^T \quad (14)$$

Equations (12) and (13) can then be written compactly as

$$\dot{\boldsymbol{x}} = f_c(\boldsymbol{x}), \qquad \boldsymbol{y} = h(\boldsymbol{x}) \quad (15)$$

where the index c is added to $f_c(\cdot)$ to discriminate the continuous-time from the discrete-time dynamics, as developed next.

B. Filter Design

For filtering, a discrete-time representation of Eq. (12) is derived by analytic integration, and disturbance terms are added:

$$\boldsymbol{x}(k+1) = f(\boldsymbol{x}(k)) + g(\boldsymbol{x}(k))\boldsymbol{w}(k), \qquad \boldsymbol{y}(k) = h(\boldsymbol{x}(k)) + \boldsymbol{v}(k) \quad (16)$$

The sampling time is $T = 1$ s throughout. The function $g(\cdot)$ maps process noise from the local frame to a body-fixed coordinate frame, such that it affects lateral and longitudinal acceleration, rather than north and east. The wind field becomes unobservable as the turn rate goes to zero; this is accounted for in the noise model by decreasing the noise gain on the wind estimate linearly with the turn rate. We therefore have

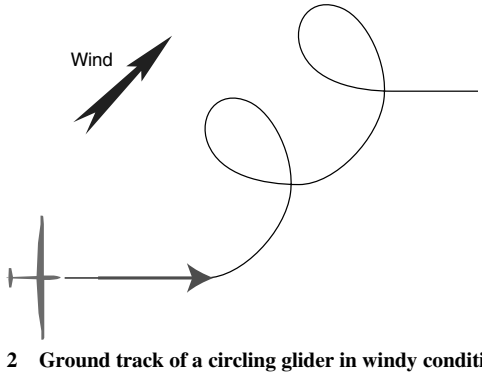

Fig. 2 Ground track of a circling glider in windy conditions.

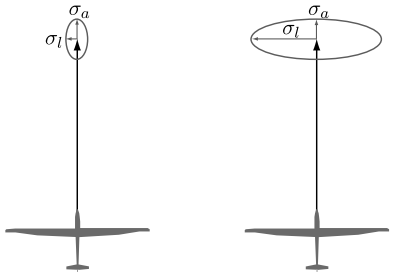

a) Uniform motion **b) Coordinated turn**

Fig. 3 Process-noise injection.

$$g(\boldsymbol{x}(k)) = \begin{bmatrix} M(\boldsymbol{x}(k)) & 0 & 0 \\ 0 & I_{2\times 2} & 0 \\ 0 & 0 & |\omega(k)|I_{2\times 2} \end{bmatrix} \tag{17}$$

with

$$M(\boldsymbol{x}(k)) = \frac{I_{2\times 2}}{\sqrt{v_E(k)^2 + v_N(k)^2}} \cdot \begin{bmatrix} -v_E(k) & v_N(k) \\ v_N(k) & v_E(k) \end{bmatrix} \tag{18}$$

essentially being a rotation matrix. An IMM filter is applied comprising both a uniform motion mode and a coordinated turn mode. The coordinated turn mode uses the full model (16) and (17), whereas the uniform motion mode employs a simplified model, fixing the turn rate to zero. Additionally, the noise covariances are chosen differently, as depicted in Fig. 3. The values for the variances and transition probabilities are determined by trial; they are given in Appendix A.

IV. Maneuver Detection

Trajectories of general aviation aircraft typically comprise a number of distinct patterns, such as cruising, circling, or random maneuvering. It is thus beneficial to detect the most frequent patterns in order to provide a better prediction accuracy. This holds true particularly for gliders, which show an even wider range of maneuvers.

The maneuver detection stage is designed to detect the most common flight patterns. It uses the turn-rate estimate $\hat{\omega}(k|k)$ determined by the state estimation stage as the input, and it employs a second IMM filter, where every mode corresponds to a maneuver. We use six modes/maneuvers, as depicted in Fig. 4. State transitions are marked by arrows. The probabilities are determined by trial and inspection of real flight data; the values are given in Appendix B.

To remain computationally feasible, the dynamic models for the six modes are kept simple; only the turn-rate dynamics are considered. More complex, albeit rare, maneuvers that involve vertical motion (e.g., a looping) are thus not captured by the algorithm. All maneuver models are given by

$$\dot{\omega}_i^M = -\frac{1}{\tau_i}(\omega_i^M - \omega_i^\infty) \tag{19}$$

for $i = 1, \ldots, 6$, and τ_i and ω_i^∞ are parameters depending on the mode. For the filter design, a discrete-time version of Eq. (19) is readily obtained. Including the process noise $w_i^M(k)$ and the measurement noise $v_i^M(k)$, we write

$$\begin{aligned} \omega_i^M(k+1) &= f_i^M(\omega_i^M(k), \omega_i^\infty) + w_i^M(k) \\ y_i^M(k) &= \omega_i^M(k) + v_i^M(k) \end{aligned} \tag{20}$$

The time constant τ_i is fixed for a given mode. The target turn rate ω_i^∞ defines the steady-state rate to which the model converges. Depending on the mode, it may vary based on past turn-rate estimates. Table 1 lists the parameters used for all modes. Note that the model for straight flight has a fixed turn rate of 0 at all times, which is indicated in the table by a time constant of 0. The symbol $\hat{\omega}_{\text{med}}$ here denotes the median of the past 10 samples of the turn-rate estimates. This formulation allows for different turn rates and turn radii in mode 5, e.g., due to different airspeeds, aircraft dynamics, or diameter of the lift area when thermaling. It assumes that the aircraft is essentially circling with a constant turn rate, but allowing for small intermittent deviations, e.g., when performing correction maneuvers to move to the center of a thermal. A minimum target turn rate is given in Table 1, such that turn rates lower than $2\pi/50$ are not considered as circling maneuvers by the filter.

The IMM filter is applied straightforwardly, where $\hat{\omega}(k|k)$ is the input. The outputs are the weighted maneuver turn rate $\hat{\omega}^M(k|k)$ and the maneuver mode probability vector $\boldsymbol{\mu}^M(k|k)$. The covariances are given in Appendix B.

V. Trajectory Prediction

The final stage of the algorithm uses outputs from the state estimation and the maneuver detection stages to produce predicted position fixes over a given horizon. Starting with the initial position $\boldsymbol{p}(k)$ obtained from the GPS, the algorithm produces consecutive position estimates $\hat{\boldsymbol{p}}(k+i|k)$ for $i = 1, \ldots, N$, where $N = 20$. Since the origin of the local coordinate frame is chosen to coincide with the position of the aircraft at every time step, we have $\boldsymbol{p}(k) = \boldsymbol{0}_{3\times 1}$. For transmission over the radio interface, the resulting trajectories are transformed back into the global reference frame.

Algorithm 1:

1) Initialize, let

$$\begin{aligned} \boldsymbol{v}_o &= [\,\hat{v}_N(k|k) \quad \hat{v}_E(k|k) \quad \hat{v}_D(k|k)\,]^T \\ \boldsymbol{d} &= [\,\hat{d}_N(k|k) \quad \hat{d}_E(k|k) \quad 0\,]^T \\ \omega_0 &= \hat{\omega}^M(k|k), \qquad \boldsymbol{p}_0 = \boldsymbol{0}_{3\times 1} \end{aligned}$$

2) Determine the maneuver mode with the highest probability:

$$m = \arg \max_{i=1,\ldots,6} \mu_i^M(k|k)$$

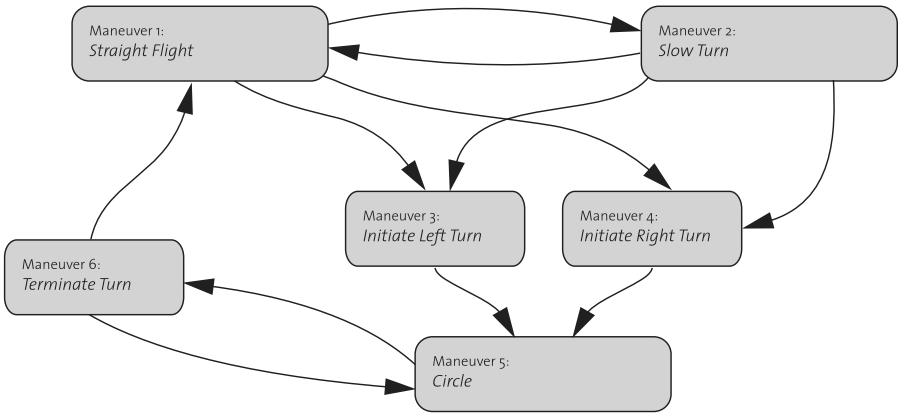

Fig. 4 Maneuver state machine used for maneuver detection.

Table 1 Filter parameters for maneuver detection stage

	Mode	Parameters	
		ω_i^∞, rad/s	τ_i, s
1	Straight flight	0	0
2	Slow turn	0	5
3	Start turn l.	$-\max\{0.25, \lvert\hat{\omega}(k)\rvert\}$	1.5
4	Start turn r.	$\max\{0.25, \lvert\hat{\omega}(k)\rvert\}$	1.5
5	Turning	$\pm\max\{\lvert\hat{\omega}_{\text{med}}(k)\rvert, \frac{2\pi}{50}\}$	1
6	Terminate turn	0	1.5

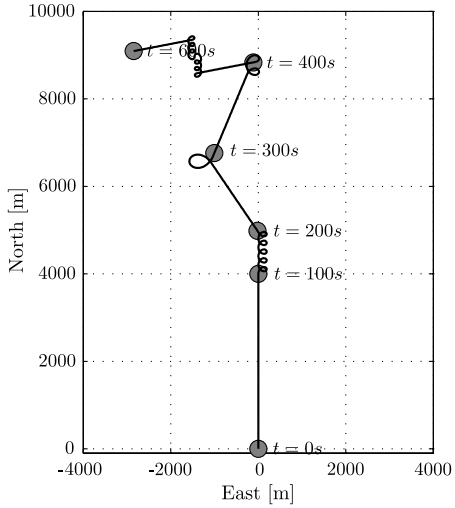

Fig. 5 Top view of simulated maneuver test sequence. Both wind speed and aircraft velocity relative to surrounding air are constant.

3) Compute future turn rates based on the current most-probable-maneuver model:

$$\omega_{i+1} = f_m^M(\omega_i, \omega_m^\infty), \qquad i = 0, \ldots, N-2$$

4) Let $\boldsymbol{\delta}_i(t) \in \mathbb{R}^6$ denote the intersampling trajectory of the aircraft relative to its position at time instant i. Solve the ordinary differential equation (ODE),

$$\dot{\boldsymbol{\delta}}_i(t) = \begin{bmatrix} 0_{3\times3} & I_{3\times3} \\ 0_{3\times3} & M(w_i) \end{bmatrix} \boldsymbol{\delta}_i(t), \qquad \boldsymbol{\delta}_i(0) = \begin{bmatrix} 0_{3\times1} \\ \boldsymbol{v}_i \end{bmatrix}$$

in the interval $t \in [0, T]$ and for $i = 0, \ldots, N-1$, where

$$M(\omega) = \begin{bmatrix} 0 & -\omega & 0 \\ \omega & 0 & 0 \\ 0 & 0 & 0 \end{bmatrix} \tag{21}$$

Set

$$\Delta \boldsymbol{p}_i = [\, I_{3\times3} \quad 0_{3\times3} \,] \boldsymbol{\delta}_i(T) \tag{22}$$

5) Compute the predicted trajectory:

$$\boldsymbol{p}_{i+1} = \boldsymbol{p}_i + \Delta \boldsymbol{p}_i + T\boldsymbol{d}, \qquad i = 0, \ldots, N-1$$

The ODE in step 4 is easily solved analytically. Specifically, step 4 can be replaced by

$$\Delta \boldsymbol{p}_i = \begin{bmatrix} \frac{\sin(T\omega_i)}{\omega_i} & -\frac{2\sin(\frac{T\omega_i}{2})^2}{\omega_i} & 0 \\ \frac{2\sin(\frac{T\omega_i}{2})^2}{\omega_i} & \frac{\sin(T\omega_i)}{\omega_i} & 0 \\ 0 & 0 & T \end{bmatrix} \boldsymbol{v}i \tag{23}$$

It should be noted that using an approximation in step 4 instead of the closed-form solution (23), e.g., the forward Euler method, will lead to an accumulation of error over the prediction horizon and is thus not recommended.

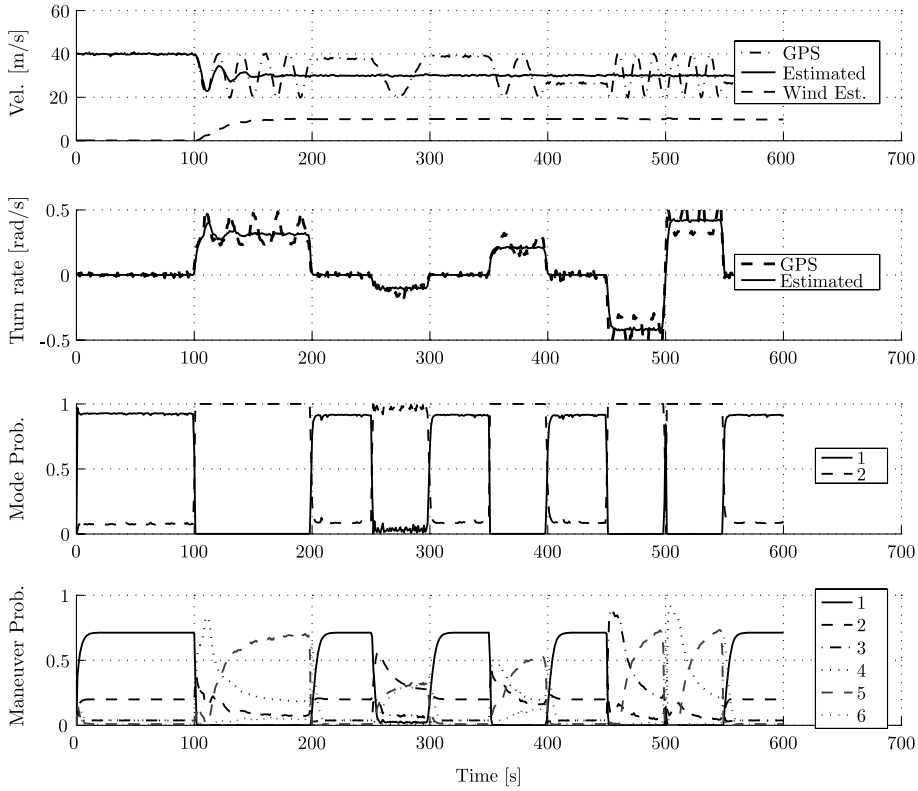

Fig. 6 Simulation result of state estimation stage, using generated flight data. In the topmost plot, GPS velocity refers to the ground speed measured by the GPS receiver. In the second plot, GPS turn rate is determined by taking the difference of two consecutive heading measurements. In the third plot, mode 1 refers to the uniform motion model, and mode 2 refers to the coordinated turn model. The maneuver numbering in the fourth plot corresponds to that given in Fig. 4.

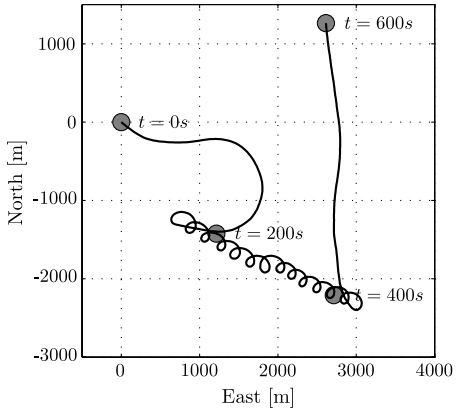

Fig. 7 Overhead plot of a real flight example on a windy day. Circling starts at $t = 130$ and continues for about 400 s. Displacement is large, due to strong wind.

The resulting trajectory $\{\boldsymbol{p}_i\}_{i=0}^{N}$ can then be converted back to the WGS-84 reference frame and transmitted using the RF transmitter.

VI. Results

The three stages of the algorithm were tuned and tested based on several data sets:

1) Synthetic data were created using a simulation model similar to Eq. (12). Various maneuvers have been included in these data, as shown in Fig. 5. A realistic amount of noise was added to the measurements.

2) Two test flights were performed on a Motorfalke airplane, using a GPS receiver with characteristics that are identical to those used in the production units. Data were recorded for later processing on the computer.

3) A database of 600 flight records adding up to more than 1700 h of flight was used for large-scale verification. These flights were typically recorded with a limited accuracy of 0.0001° for latitude/longitude and with a time interval of 1 or 2 s. Furthermore, only position fixes were recorded; no velocity measurements were available. To attain a similar level of fidelity, the data were preprocessed and missing data were reconstructed using a spline algorithm.

A simulation result for the state estimation stage is shown in Fig. 6. The filter is initialized with a (wrong) wind estimate of zero. It can be observed that this error leads to oscillation of the turn rate when the aircraft starts circling for the first time. The wind estimate then converges to the true wind speed in less than three full circles.

A challenging but realistic situation for the algorithm is depicted in Fig. 7. These data have been extracted from one of the flights in the database. It shows a real situation that a glider pilot encountered during a windy day with weak thermals. Filter output for this example is depicted in Fig. A1. It can again be observed the wind estimate converges in about three full circles.

To assess the prediction accuracy that can be expected in real-world scenarios, the algorithm was applied to the flights in the database. By comparing the true position at time $k + i$ as measured by the GPS receiver with the i-step prediction at k, the prediction error was quantified directly for each individual flight record and for varying prediction times i. The rms of the prediction error was then computed, yielding a combined statistical measure of the accuracy of the trajectory prediction. Results are shown in Fig. A2. For reference, the performance of the legacy algorithm is also shown.

To assess the sensitivity of the filter to wind, the flight records from the database were categorized into calm-wind, medium-wind, and strong-wind conditions. The calculation of rms prediction errors was repeated for each of these subsets, and the results are depicted in Fig. A3. It can be seen that the new algorithm offers better accuracy

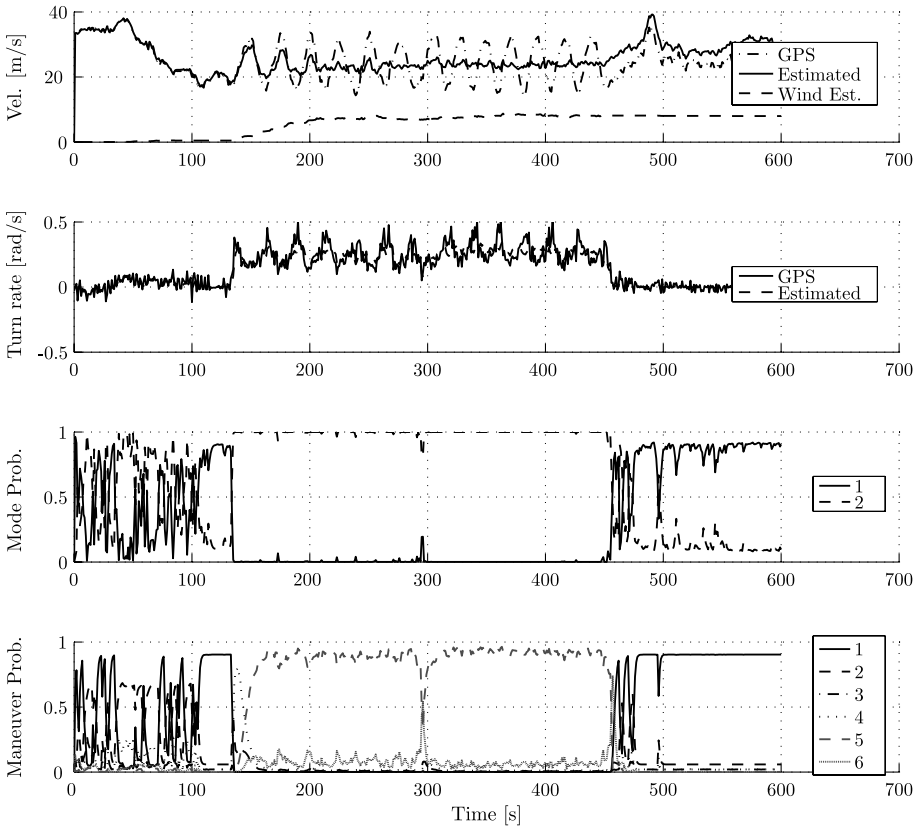

Fig. A1 Filter output for real flight example. Filtered outputs are shown for estimation and maneuver detection stages. The filter is initialized with a wind speed of zero. Once circling starts (at $t = 130$ s), the wind estimate converges within about 1 min. The oscillations in estimated airspeed and turn rate are decreased significantly.

over almost the whole prediction horizon. More important, the results show little-to-no sensitivity to wind, yielding almost the same performance on windy days as on calm days.

VII. Conclusions

A novel algorithm has been proposed for trajectory prediction of light aircraft. The algorithm is designed for employment in the low-cost traffic advisory and collision avoidance system FLARM. It has been validated and tested on both simulated and real flight data on a large scale. It almost always provides more accurate predictions than the legacy algorithm, independently of maneuvers and wind. The improvement is particularly significant in windy conditions, where the new algorithm does not show any sensitivity to wind in a statistical sense. The algorithm will be implemented in production units in 2010/2011.

Appendix A: Process Parameters for State Estimation

The noise covariances used in the state estimation filter are given by

$$Q_i = \mathrm{diag}([\,\sigma_l \quad \sigma_a \quad \sigma_D \quad \sigma_\omega \quad \sigma_w \quad \sigma_w\,]) \tag{A1}$$

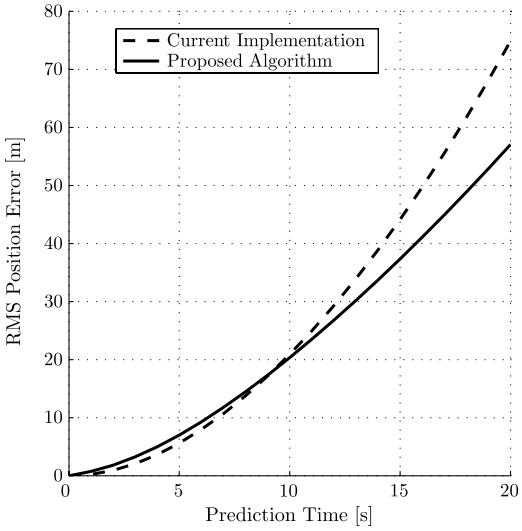

Fig. A2 Root-mean-square prediction-error comparison in cruise flight of legacy filter to proposed filter; 600 flights were processed.

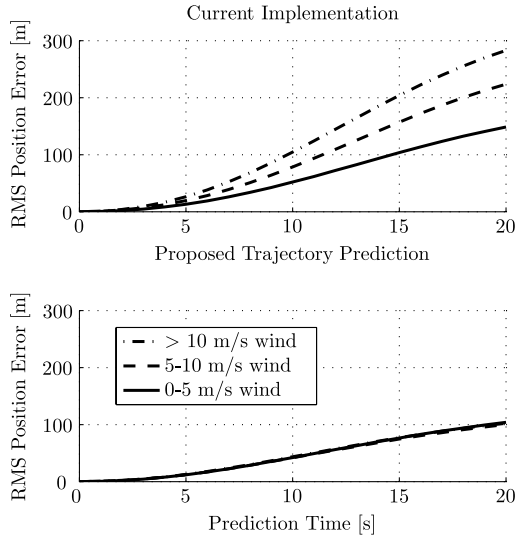

Fig. A3 Statistical comparison of wind sensitivity of legacy to proposed filter. The new filter does not show any susceptibility to wind with regard to prediction accuracy.

Table A1 Process-noise variances used in the state estimation stage[a]

Mode	σ_l, g	σ_a, g	σ_d, g	σ_Ω, deg/s^2	σ_w, g
$i=1$	0.02	0.1	0.02	0	0
$i=2$	0.25	0.12	0.02	4	0.1

[a]Earth's gravitation is denoted by g.

Table A2 Measurement noise variances used in the state estimation stage

Parameter	Value, m/s
σ_N	1
σ_E	1
σ_D	2

Table B1 Maneuver detection model parameters[a]

Mode	Q_i^M, deg/s^2	R_i^M, deg/s
1	3	1
2	5	1
3	5	1
4	5	1
5	5	1
6	5	1

[a]$Q_i^M = E[w_i^M(t)^2]$ and $R_i^M = E[v_i^M(t)^2]$.

$$R_i = \mathrm{diag}([\,\sigma_v N \quad \sigma_v E \quad \sigma_v D\,]) \tag{A2}$$

for each individual node, with $i \in \{1, 2\}$. Mode 1 is the uniform motion mode, and mode 2 is the coordinated turn mode. The particular values for the parameters are found by trial and error and are given in Tables A1 and A2. The transition probabilities of the underlying Markov chain are given by

$$P = \begin{bmatrix} 0.8 & 0.2 \\ 0.1 & 0.9 \end{bmatrix} \tag{A3}$$

Appendix B: Process Parameters for Maneuver Detection

The noise covariances for the maneuver detection filter are given in Table B1. The transition probabilities of the underlying Markov chain are given by

$$P^M = \begin{bmatrix} 0.7 & 0.1 & 0.1 & 0.1 & 0 & 0 \\ 0.1 & 0.8 & 0.05 & 0.05 & 0 & 0 \\ 0 & 0.08 & 0.8 & 0.02 & 0.1 & 0 \\ 0 & 0.08 & 0.02 & 0.8 & 0.1 & 0 \\ 0 & 0 & 0 & 0 & 0.8 & 0.2 \\ 0.05 & 0.05 & 0.03 & 0.03 & 0.04 & 0.8 \end{bmatrix} \tag{B1}$$

Acknowledgments

This work would not have been possible without the help and support by FLARM Technology, Ltd., which provided the authors with experimental setups and with privileged access to confidential information. We also thank the anonymous reviewers; their suggestions have helped to improve the quality of the paper substantially.

References

[1] Larpin, R., "Mid-Air Collisions," Federal Department of Environment, Transport, Energy and Communication, Federal Office of Civil Aviation, Bern, Switzerland, Nov. 2003.

[2] Bureau, A. T. S., "Limitations of the See-and-Avoid Principle," Australian Transport Safety Bureau, Canberra, ACT Australia, 1991.

[3] Bar-Shalom, Y., Li, X. R., and Kirubarajan, T., *Estimation with Applications to Tracking and Navigation*, Wiley, 605 New York, 2001.

[4] Sorenson, H. W., "Approximate Solutions of the Nonlinear Filtering Problem," *IEEE Conference on Decision and Control*, Vol. 16, Dec. 1977, pp. 620–625.

[5] Denham, W. F., and Pines, S., "Sequential Estimation When Measurement Function Nonlinearity is Comparable to Measurement Error," *AIAA Journal*, Vol. 4, No. 5, Aug. 1966, pp. 1071–1076. doi:10.2514/3.3606

[6] Magill, D., "Optimal Adaptive Estimation of Sampled Stochastic Processes," *IEEE Transactions on Automatic Control*, Vol. 10, No. 4, Oct. 1965, pp. 434–439. doi:10.1109/TAC.1965.1098191

[7] Blom, H. A. P., "An Efficient Filter for Abruptly Changing Systems," *23rd IEEE Conference on Decision and Control*, Vol. 23, IEEE, Piscataway, NJ, Dec. 1984, pp. 656–658.

[8] Blom, H. A. P., and Bar-Shalom, Y., "The Interacting Multiple Model Algorithm for Systems with Markovian Switching Coefficients," *IEEE Transactions on Automatic Control*, Vol. 33, No. 8, Aug. 1988, pp. 780–783. doi:10.1109/9.1299

[9] Bar-Shalom, Y., Chang, K. C., and Blom, H. A. P., "Tracking a Maneuvering Target Using Input Estimation Versus the Interacting Multiple Model Algorithm," *IEEE Transactions on Aerospace and Electronic Systems*, Vol. 25, No. 2, March. 1989, pp. 296–300. doi:10.1109/7.18693

[10] Nabaa, N., and Bishop, R. H., "Validation and Comparison of Coordinated Turn Aircraft Maneuver Models," *IEEE Transactions on Aerospace and Electronic Systems*, Vol. 36, No. 1, Jan. 2000, pp. 250–259. doi:10.1109/7.826327

[11] Maybeck, P. S., Worsley, W. H., and Flynn, P. M., "Investigation of Constant Turn-Rate Dynamics Models in Filters for Airborne Vehicle Tracking," *Proceedings of the IEEE National Aerospace and Electronics Conference*, IEEE, Piscataway, NJ, 1982, pp. 896–903.

[12] Watson, G. A., and Blair, W. D., "IMM Algorithm for Tracking Targets that Maneuver Through Coordinated Turns," *Proceedings of SPIE*, Vol. 1698, Nos. 20–22, 1992, pp. 236–247. doi:10.1117/12.139376

[13] Bar-Shalom, Y., and Li, X. R., *Estimation and Tracking: Principles, Techniques, and Software*, Artech House, Norwood, MA, 1993.

[14] Blackman, S., and Popoli, R., *Design and Analysis of Modern Tracking Systems*, Artech House, Norwood, MA, 1999.

[15] Bar-Shalom, Y., and Blair, W. D., *Multitarget-Multisensor Tracking: Applications and Advances*, Vol. 3, Artech House, Norwood, MA, 2000.

[16] Bishop, R. H., and Antoulas, A. C., "Nonlinear Approach to Aircraft Tracking Problem," *Journal of Guidance, Control, and Dynamics*, Vol. 17, No. 5, Sept.–Oct. 1994, pp. 1124–1130. doi:10.2514/3.21319

[17] Wang, H., Kirubarajan, T., and Bar-Shalom, Y., "Precision Large Scale Air Traffic Surveillance Using IMM/Assignment Estimators," *IEEE Transactions on Aerospace and Electronic Systems*, Vol. 35, No. 1, Jan. 1999, pp. 255–266. doi:10.1109/7.745696

[18] Mazor, E., Averbuch, A., Bar-Shalom, Y., and Dayan, J., "Interacting Multiple Model Methods in Target Tracking: A Survey," *IEEE Transactions on Aerospace and Electronic Systems*, Vol. 34, No. 1, Jan. 1998, pp. 103–123. doi:10.1109/7.640267